Journal of Physics:
Conference Series

PAPER • **OPEN ACCESS**

Field experiments of wind turbine vibrations in stand still conditions

To cite this article: Johan Peeringa *et al* 2025 *J. Phys.: Conf. Ser.* **3131** 012013

Journal of Physics: Conference Series **3131** (2025) 012013 doi:10.1088/1742-6596/3131/1/012013

Field experiments of wind turbine vibrations in stand still conditions

Johan Peeringa[1], Erik Fritz[1], Feike Savenije[1], Koen Boorsma[1], Andreas Herrig[2] and Max Bouwmeesters[3]

[1]TNO
[2]LM Wind Power (now at GE Vernova)
[3]Former TU Delft master student and intern at TNO

E-mail: johan.peeringa@tno.nl

Abstract. Modern wind turbines become increasingly flexible, and as a result more sensitive to vibrations. Currently, wind turbine vibrations at standstill are observed at high wind speeds. However, the exact conditions and sources of excitation causing the vibrations are not sufficiently understood.

Dedicated field experiment were executed, utilizing a parked 3.8 MW research turbine to identify these conditions. To trigger vibrations of the wind turbine, a dedicated test at different pitch and yaw angles and rotor positions was performed at standstill. The measurements were done for wind speeds of at least 15 m/s.

During the experiment, blade root bending moments are measured together with surface static pressure distribution measurements at a cross section 15 m from the blade root. In addition to that, tower bending moments and accelerations are measured.

The experimental data is analyzed first to identify the vibration modes and the associated conditions. To assist in this identification, wind turbine simulations are performed. The numerical studies confirm the need for realistic turbulent inflow conditions and a good dynamic stall model.

1 Introduction

Over the past few decades, wind turbines have shown a trend to become increasingly larger. This resulted in very long and slender blades becoming more sensitive to vibrations at lower frequencies. It is during standstill or idling conditions that turbine blades may experience high angles of attack when two distinct phenomena might occur: Stall-induced Vibrations (SiV) and Vortex-induced Vibrations (ViV). At its core, stall-induced vibrations relate to the variation of lift L and drag D forces with a varying angle of attack α. As explained by Den Hartog [1] this can cause an unstable system in case a negative slope of the lift is greater than the drag force $\frac{\partial L}{\partial \alpha} + D < 0$. The aerodynamic damping has become negative, and excites any already existing oscillation [2].

The conditions for Vortex-induced vibrations on a body are described by Fung [3] as follows "The frequency of the wake vortices is determined by the geometry of the body and the speed of the flow. If the frequency is close to the natural vibration frequency of the body, resonance will set in."

A literature study on SiV and ViV by Bouwmeesters [4] shows most of the research was purely based on numerical simulations. Exceptions to this are for ViV in a wind tunnel experiment [5] and a study into SiV which used an on-site turbine as validation [6]. There is a lack of experimental data from in-field

tests for different yaw and pitch angles and azimuth positions. This article fills this gap using a full-scale on-site testing turbine for analysis of VIV and SIV.

In Section 2 the experiment is discussed in detail. Vibration modes, frequency and damping, are identified for the wind turbine system first. In two experiments actual vibrations of the wind turbine are observed. For these cases the pressure data are analyzed.

Wind turbine designs are based on simulations as defined in the IEC 61400-1 standard [7]. Nevertheless severe vibrations are observed in the field during standstill. Also instabilities sometimes occur in design calculations but not in reality. In Section 4 simulations performed with the in-house linear time-invariant aeroelastic tool TURBU are described.

The paper closes with conclusions and recommendations for future work.

2 Experiment setup and test conditions

In the TIADE project, a large number of different experiments were accomplished. To support these the test turbine was heavily instrumented. A concise description of the instrumentation will be presented, followed by an explanation of the dedicated ViV and SiV campaigns.

The set-up of the experiment involves the TIADE fullscale prototype turbine. Two out of three blades are equipped with strain gauges near the root, allowing the estimation of the edge- and flap-wise bending moments as shown in the cross-section in Figure 1. The blades equipped with these strain gauges are blades number 2 and 3.

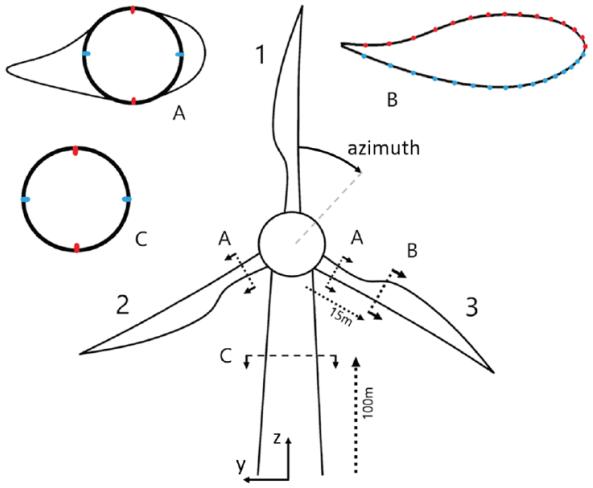

Figure 1: Front view of the turbine set-up, with the azimuth angle defined clockwise from the position straight up [4]. Cross-section A: strain gauges in blade root; Cross-section B: pressure sensors in blade 3; Cross-section C: strain gauges in the tower.

The pressure distribution around the blade cross-section at 25 % of the blade radius is measured using 31 static pressure taps. Each tap measures the differential pressure between the blade surface and a reference pressure measured in the turbine hub. A 38 % thick airfoil, which is similar to the DU-00-W-401 airfoil, defines the blade contour at the measurement location. Figure 2 schematically shows the pressure measurement setup and the naming convention used to describe the sensors. For a more detailed discussion of the test site and measurement setup the reader is referred to Fritz et al. [8].

To obtain the environmental data, there are three sources of information. First of all, a wind measuring station on the nacelle which can obtain the wind speed and direction. Secondly, a met mast approximately 1.5 km away which can provide further information on the atmospheric stability. And lastly, a profiling lidar 280 meters upwind (in the predominant wind direction) of the wind turbine. The direction from tower w.r.t. North is 210°. The lidar was used to determine the inflow wind velocities at the following altitudes: 42, 58, 71, 82, 97, 110, 121, 136, 162, 175 and 188 m. These various options are sketched in Figure 3.

The met mast is located relatively far away, which can give a decent indication of the current atmospheric conditions, but will not result in accurate wind speed estimates. Hence during this project, the profiling lidar upwind of the wind turbine is used as the main source of inflow data.

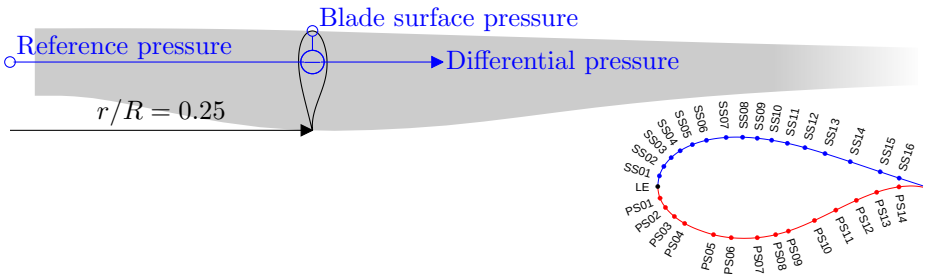

Figure 2: Schematic of the measurement setup and airfoil contour with pressure taps (including the sensor naming convention)

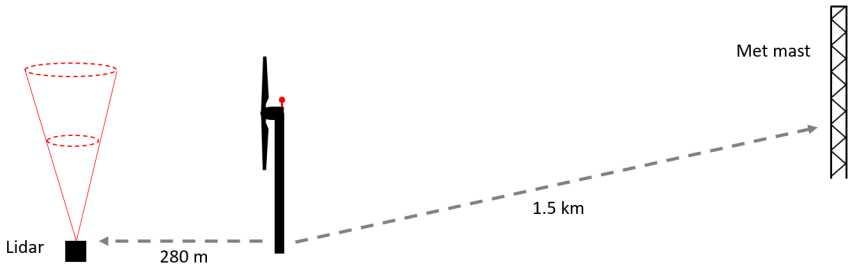

Figure 3: Wind measurement set-up (not to scale): nacelle anemometer, lidar 280 m upwind, met mast 1.5 km away [4]

An overview of the test campaigns is given in Table 1 where the operational conditions are listed in terms of the three blades' pitch angles, the yaw misalignment angle, the rotor azimuth, the wind speed (and its standard deviation), the turbulent intensity TI and the wind direction.

Table 1: Test campaigns run during the SiV and ViV experiment (varied parameter in bold font)

#	**Pitch** [°] Blade 1	Blade 2	Blade 3	**Yaw mis.** [°]	**Azimuth** [°]	**Wind (std)** [m/s]	**TI** [%]	**Wind dir.** [°]
1	85	**[-15,85]**	85	0	120	15.9 (2.0)	13	290
2	85	85	**[-15,165]**	0	240	14.3 (1.6)	11	150
3	85	**[85,180]**	85	90	120	18.8 (2.6)	14	265
4	85	85	85	**[0,60]**	120	15.9 (2.0)	13	290
5	85	85	85	**[-130,95]**	240	14.3 (1.6)	11	150
6	85	85	85	**[-5,200]**	240	19.1 (2.6)	14	242
7	85	85	85	**[-110,90]**	330	17.4 (3.4)	19	270
8	85	180	85	**[94,113]**	120	19.5 (2.8)	14	270
9	85	85	180	**[117,94]**	240	16.6 (1.8)	11	268
10	89	89	89	90	**[240,360]**	19.2 (2.6)	14	256

Experiments 8 and 9 are unique, because during these experiments severe vibrations were visibly present in the wind turbine. The effect of SiV and ViV is less noticeable in the other experiments, but there are still a few conditions identified, where oscillations in the measured forces tend to increase in magnitude.

3 Experimental results

The experimental results are used to analyze the structural response and possible vortex shedding as a source of excitation. A spectral analysis is applied on the strain gauge measurements to investigate the structural behaviour. Separation on a blade section is studied using pressure sensors data. Next the extreme SiV and ViV campaings are analyzed.

3.1 Response analysis

The first step in analyzing the data is to identify the dominant frequencies. These frequencies were identified purely by inspection of the spectral distributions of the various force measurements. Most frequencies were validated using an internal TNO report [9]. The frequencies have been normalized with respect to the 1st tower mode. All natural frequencies were obtained by identifying the peaks in the power spectral density (PSD) plots created from the measured data of the turbine.

The structural behavior of the blade frequencies appears to be strongly coupled with their relative position/pitch angle. Varying the pitch of a single blade not only affects the aerodynamic damping of the turbine but also the structural frequencies to which it is sensitive. Figure 4 compares the force oscillations for the local angle of attack for blade 3 caused by either changing pitch or yaw angle.

When all blades are pitched by 85° and the yaw angle is 0°, both the pitch traverse and yaw traverse are the same conditions and angle of attack (AoA). However, for any other angle of attack, the pitch and yaw traverse experience the same flow over the top blade (at 0° azimuth), but experience different conditions over the remaining blades and nacelle. In Figure 4 it is seen that the pitch traverse causes some of the blade's excited modes to shift, while for the yaw traverse, they remain at a constant frequency. The normalized tower frequencies at 1 and 7.9 do not appear to shift due to the pitch traverse. For the edgewise bending moment, the peak of the asymmetric edgewise mode in tilt becomes more broad and ends up merging with the symmetric edgewise mode. During the yaw traverse these edgewise modes remain quite narrow. There are also some peaks present in the pitch traverse which are not visible during the yaw traverse. This becomes more clear in Figure 5 where the power spectrum is plotted for the edgewise bending moment for angles of attack of 5° and 55°. At 55° angle of attack, there are three additional modes visible in the pitch traverse: the rotor shaft, the edgewise asymmetric mode, and a flapwise/edgewise coupled mode. Also, the shifting peaks are observed.

The pressure data is now analyzed for the occurrence of periodic vortex shedding, which can cause vortex-induced vibrations. Such periodic vortex shedding can be characterised by the Strouhal number

$$St = \frac{f\, L_{proj}}{U} \ , \tag{1}$$

where f is the vortex-shedding frequency and L_{proj} is the length of the airfoil projected onto the plane perpendicular to the inflow velocity U. From existing literature, it is expected that an airfoil's Strouhal number is slightly lower than that of a cylinder. Therefore, a range of $St = 0.16...0.2$ is chosen to calculate a range of frequencies in which the vortex-shedding frequency is expected [10].

To investigate whether periodic vortex shedding occurs, the frequency spectra of the pressure measurements and, in the case of partial flow separation, the spectrum of the separation point location are analyzed. The flow separation results in a flattened pressure distribution and, thus, in a very low chordwise pressure gradient $\frac{\partial p}{\partial x/c}$ in the separated region of the airfoil. Based on this observation, the separation point can be estimated by fitting two lines through the measured pressure values, one through the attached region with steep pressure gradient and one through the separated region. This methodology is schematically shown in Figure 6 (a). The resulting time series of the estimated separation point location is plotted in Figure 6 (b). It can be observed that considerable changes occur in the amount of separation, with an onset varying between approximately 10 % and 40 % chord. However, analyzing the frequency content of the estimated separation point location's signal does not reveal a clearly identifiable vortex-shedding frequency, see Figure 6 (c).

3.2 Extreme SiV and ViV campaigns

Test campaign 8 yielded vibrations with increasing magnitude so that the test had to be stopped to ensure the turbine's safety. This campaign was characterized by yaw misalignment angles of approximately 90° to 120° with blade 2 pointing vertically upward. This upward-facing blade was rotated to a pitch angle of 180° while the two lower blades were pitched to vane (85°). Test campaign 9 was a repeat of campaign 8 but with blade 3 (the blade instrumented with pressure sensors) instead of blade 2 pointing upwards. It should be noted that for both campaigns, the combination of yaw misalignment and pitch angles entails that the airfoil's trailing edge points towards the inflow velocity, contrary to the way an airfoil is oriented in regular operation. Nonetheless, regular naming conventions are adhered to so that the leading edge refers to the airfoil's rounded end, while the trailing edge refers to the sharp end of the airfoil.

Figure 7 shows various measurement signals, where the left column represents test campaign 8 and the right column test campaign 9. The yaw misalignment angle is plotted in Figure 7 (a) and (b), the flapwise blade root bending moment in Figure 7 (c) and (d), and the edgewise blade root bending moment in Figure 7 (e) and (f).

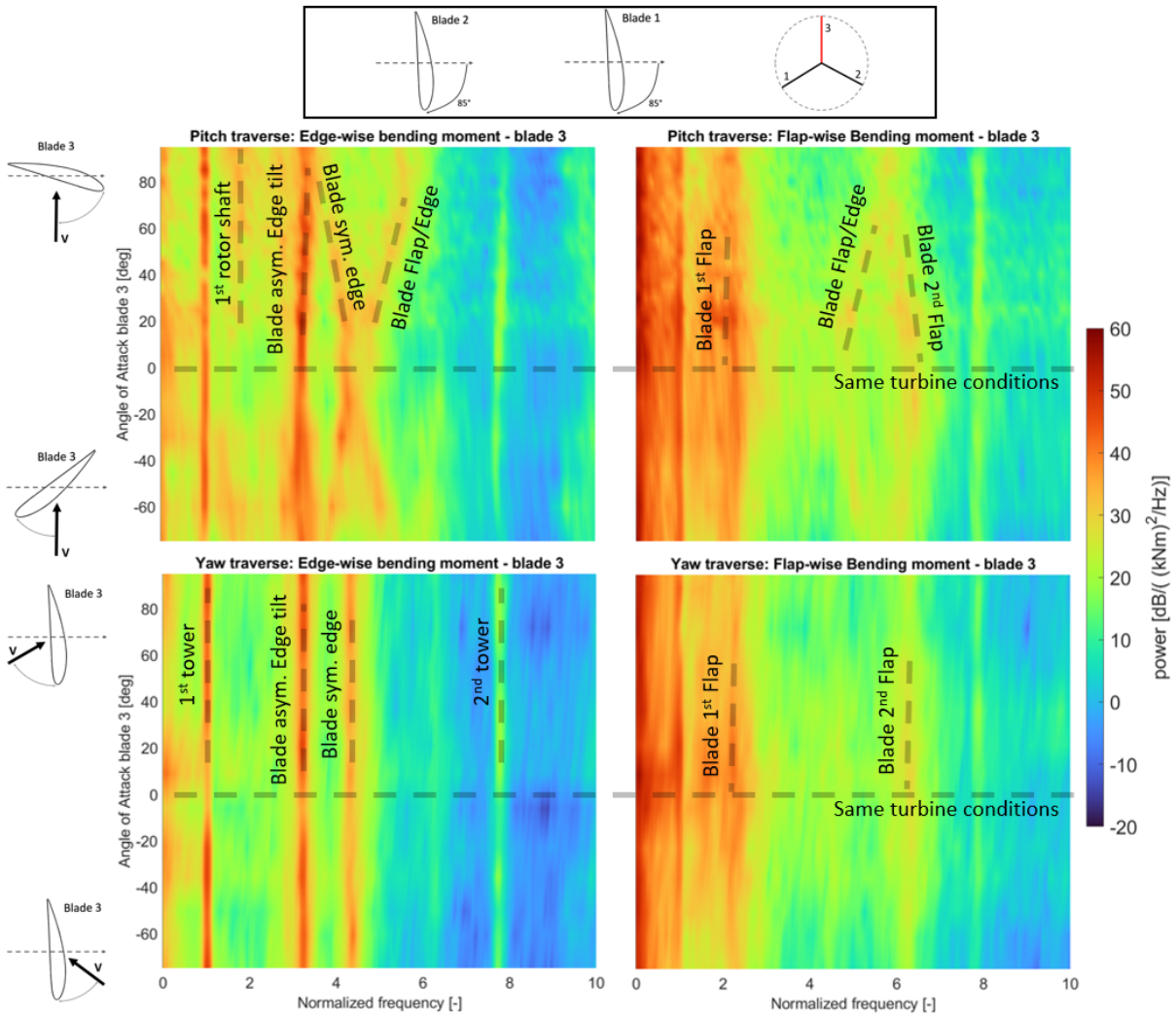

Figure 4: Blade flapwise and edgewise bending moment vs angle of attack, for both a pitch traverse test campaign 2 (top) and a yaw traverse test campaign 5

It is evident that the wind turbine experienced self-excited vibrations during campaign 8. Eventually, the increasing vibration magnitude was considered unsafe and the pitch angle was reduced to 120° effectively returning the vibrations to a damped state. While test campaign 9 did not experience vibrations with as clearly increasing amplitude as during campaign 8, strong vibrations still occurred so the pressure measurements can offer valuable insights into the underlying aerodynamics.

The mean pressure distributions for three different yaw misalignment angles in test campaign 9 are shown in Figure 8. Additionally, error bars indicate the range of plus/minus one standard deviation of the underlying pressure data from the mean. As mentioned above, the airfoil's trailing edge points approximately towards the inflow velocity for the considered cases. This leads to unconventional pressure distributions exhibiting the widest spread between pressure and suction side close to the trailing edge.

While the case with yaw angle 93.1°, see Figure 8 (a), still has a non-zero pressure gradient on the suction side of the airfoil (blue line), the pressure distribution flattens out with increasing yaw angle. This indicates that for these higher yaw angles, the flow on the airfoil's suction side separates increasingly. This is also supported by the reducing standard deviation. For yaw angle 93.1°, the flow is likely attached and slight changes in the wind direction, and the consequent change in angle of attack, will lead to changes in the suction level. For yaw angle 118.4°, see Figure 8 (c), the flow separation entails that the pressure level along the suction side changes less, which shows in the much smaller standard deviation. The pressure side measurements (red line) are affected far less by the changes in yaw misalignment than the suction

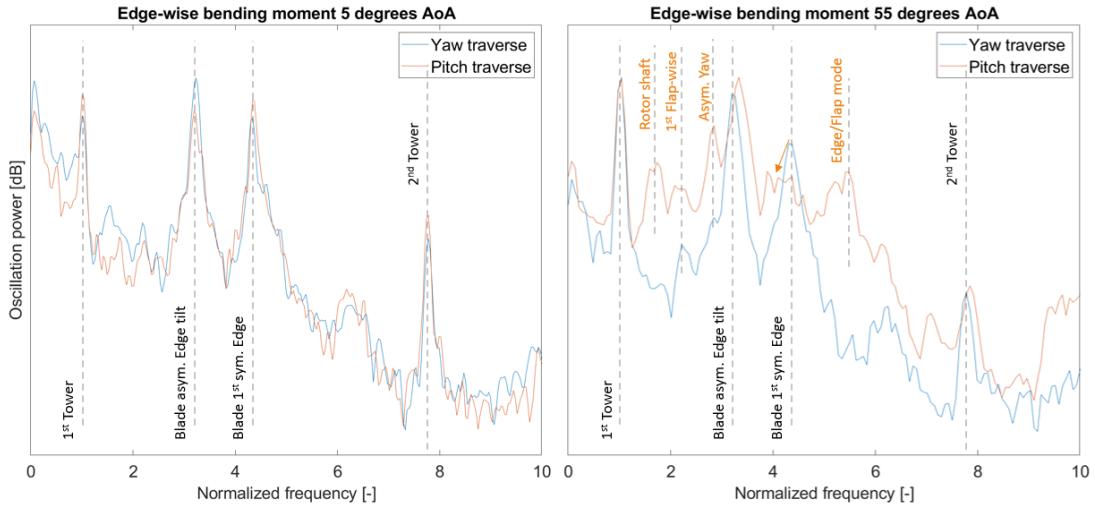

Figure 5: Edgewise bending moment at 5° and 55° angle of attack, for both a pitch traverse and a yaw traverse

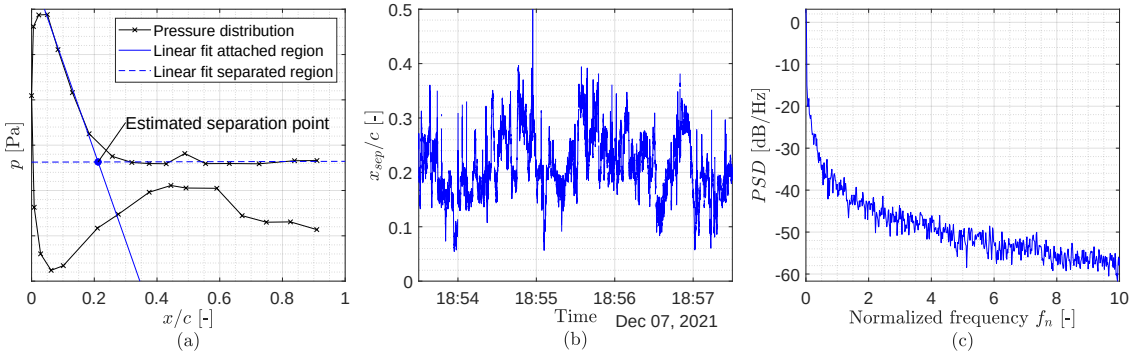

Figure 6: Schematic of the separation point determination (a), estimated separation point location as a function of time (b) and PSD of the separation point location signal (c)

side measurements.

Figure 9 (a) and (b) shows the frequency spectra of the selected pressure sensors for the case with yaw angle 93.1°, while Figure 9 (c) shows a schematic of the inflow conditions. In this yaw misalignment, the inflow velocity is close to aligned with the chord line. Based on the mean measured inflow velocity during this period and the projected length of the airfoil in the plane perpendicular to the inflow, the vortex-shedding frequency normalized by the first tower frequency is expected to lie in the range of $f_{n,exp} = 7.69..9.56$. The spectra of most sensors do not exhibit any clear peaks, resulting in spectra comparable to that of sensors PS10 given in Figure 9 (b). Contrastingly, a peak can be observed for sensors SS06 - SS11 at approximately $f_n = 7.54$, exemplary shown for SS10 in Figure 9 (a).

The current experimental setup makes it difficult to derive with certainty a causality between different observations. Neither does the presence of a vortex-shedding frequency mean that vortex-induced vibrations occurred, nor does the lack of the identified vortex-shedding frequency in the blade root bending moment spectra mean that no vortex-induced vibrations occurred.

4 Aeroelastic simulation

4.1 Introduction

Prediction of potential vibration issues with operational and standstill wind turbines using aero-elastic models can be valuable to detect problems early in the design phase, but is also challenging due to their complex dynamic behavior. A common approach to address this is to perform a stepwise analysis using

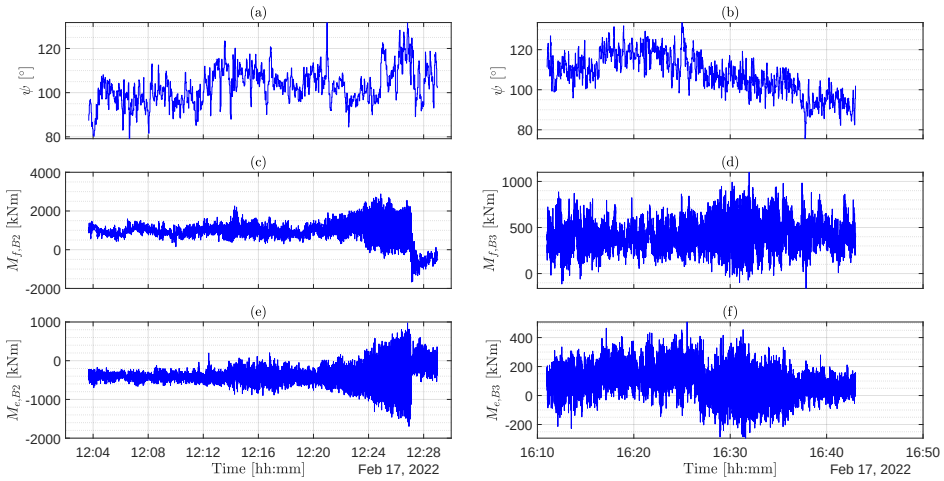

Figure 7: Signals of yaw misalignment angle ψ (a) and (b), flapwise blade root bending moment M_f (c) and (d), and edgewise blade root bending moment M_e (e) and (f) during the extreme vibration cases; left column represents test campaign 8, right column test campaign 9

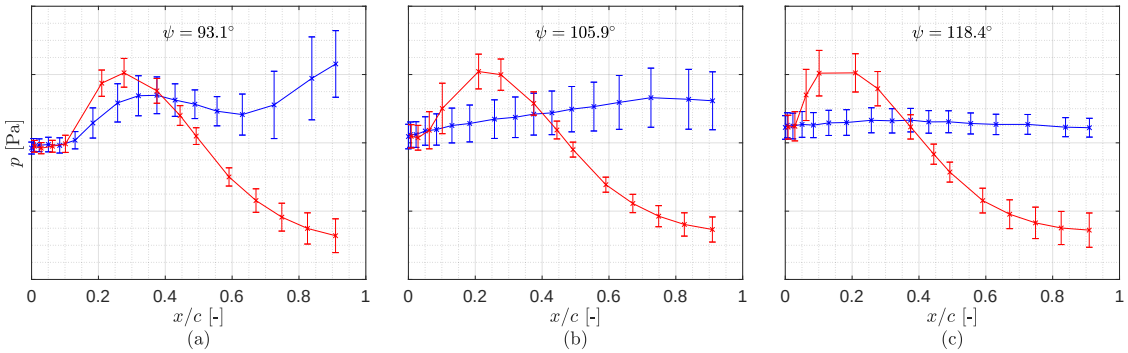

Figure 8: Mean pressure distributions for three different yaw misalignment angles; blue: measurements on suction side, red: measurements on pressure side; error bars represent one standard deviation

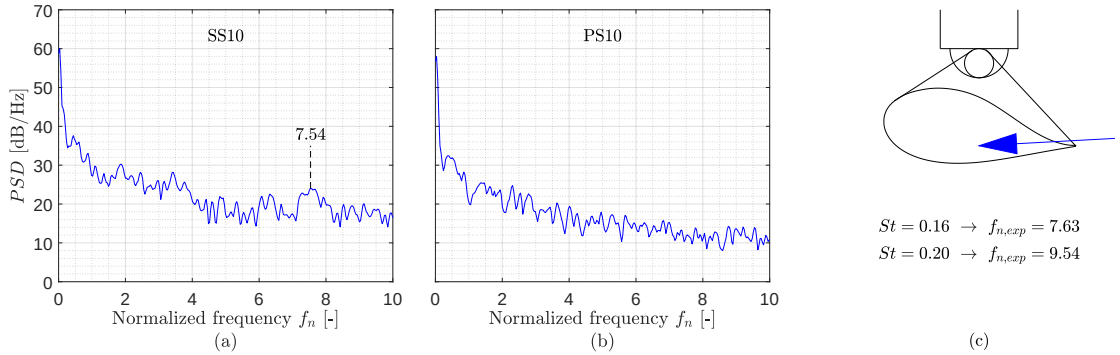

Figure 9: Power spectral density of pressure sensors SS10 (a) and PS10 (b) for a yaw misalignment angle of $\psi = 93.1°$, a schematic of the inflow direction and expected vortex shedding frequency range in (c)

models of different fidelity. These range from low order frequency domain methods, across non-linear time domain methods to (coupled) CFD analysis. The low order models are least expensive, and can support

the analysis with scoping the often large range of environmental and operating conditions. Based on the design documentation of the research wind turbine and various other sources, a set of models has been prepared and verified/validated using measurements [4, 9]. Among other checks, a close match of natural frequencies of the blades and the tower is observed. This section describes the scoping of first order stability across the range of standstill conditions using the aero-elastic model TURBU, with attention to the stall region.

4.2 Method

The stability analysis in this section makes use of the linearized frequency and time domain method TURBU [11, 12]. TURBU exploits the rotational symmetry of a three-bladed horizontal axis wind turbine to derive a linear time-invariant model using the Coleman transform. TURBU calculates the equilibrium state for a given operating point and provides an analytically linearized wind turbine model for that condition. Model reduction can be performed to limit the amount of states, both on the aerodynamic (number of stream tube annuli) and the structural dynamic (number of modes) side. The resulting reduced-order linear model can be used for controller synthesis, design iterations and load case scoping. The linearization produces structured state-space matrices, which can be stacked to cover all operating points. A linear version of the Snel dynamic stall model [13] is included.

4.3 Results

Two standstill experiments with pitch and yaw sweep as described in Section 2 are performed numerically, using the model derived with TURBU. This section contains results for the blade pitch angle sweep from power to feather and beyond ($0 \rightarrow 160°$, blade tip angle of attack range $90 \rightarrow -60°$). The test conditions also include zero yaw misalignment, high ($\sim$20 m/s) wind speed and brake applied. Note that, other than in the experiment, the pitch sweep is applied to all the blades for this numerical analysis. The results are normalized with respect to the frequency of the first tower bending mode.

Figure 10 shows the modal frequency and damping results for the pitch sweep. Several modes show large shift in frequency when moving through the sweep, which indicates the importance of component interaction. Also the damping values change significantly for some of the modes, which can be attributed to influence of aerodynamic forcing. This overview is very useful to identify areas of interest; while low or even negative values of modal damping indicate potential stability issues, resonance can occur when excitation frequency is close to natural frequencies (e.g. linked to nP harmonics of rotation, or vortex shedding in the standstill case). Some areas for further investigation are identified:

- Negative damping for the (set of) blade first flatwise modes ($f_n \approx 2$) between $60 - 90°$ pitch angle; this is linked to stall behavior with negative $\mathrm{d}c_l/\mathrm{d}\alpha$ at high[1] wind speeds (in short: forward motion of the blade $\rightarrow$ backward velocity component $\rightarrow$ angle of attack increase $\rightarrow$ backward force reduction $\rightarrow$ forward motion increase $\rightarrow$ etc)
- Negative damping for the collective drive train mode with blades in feather (similar mechanism as above, but with all blades and the shaft involved)
- Potential resonance due to vortex shedding for several modes, indicated with dashed lines representing estimates of the excitation frequency based on Strouhal number (see Equation 1 in Section 3.1)

To assess the importance of these potential issues under realistic conditions, spectral analysis or time domain simulations can be performed with TURBU. Figure 11 shows the power spectral density contour (psdc) for the edgewise blade root bending moment. In comparison to the experimental results shown in Figure 4, similar trends are observed. The effect of the drive train mode at $f_n \approx 2$ is more pronounced due to the pitching of all blades, especially for large AoA ($> 50°$) with all blades pitching to work position and very little damping from aerodynamic forcing on the drive train mode. The psdc for the flatwise blade root bending moment in Figure 11 is in quite good agreement with the experimental data shown in Figure 4, both for the behavior at the first ($f_n \approx 2$) and the second ($f_n \approx 6$) flatwise bending modes. The low damping region ($\alpha \approx 15°$) stands out, both in the numerical and the experimental results.

As the stall region appears challenging from both modal and spectral analysis, this asks for zooming in on the low frequency modes and the pitch range of interest. Figure 10 shows their modal frequency and damping, with negative damping values for both the tower and the blade dominated modes.

[1] At low wind speeds, the decrease of force due to AoA change will be countered by the increase of force due to the increase of effective velocity from motion. With the current model, the negative damping reduces to $\sim$10% for 8 m/s average wind speed.

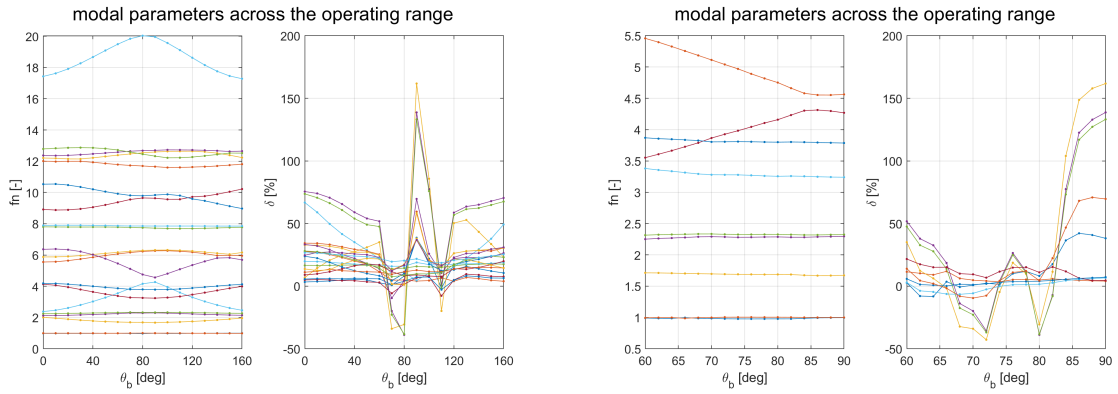

Figure 10: Modal frequency and damping for the pitch sweep full range (left) and zoomed (right)

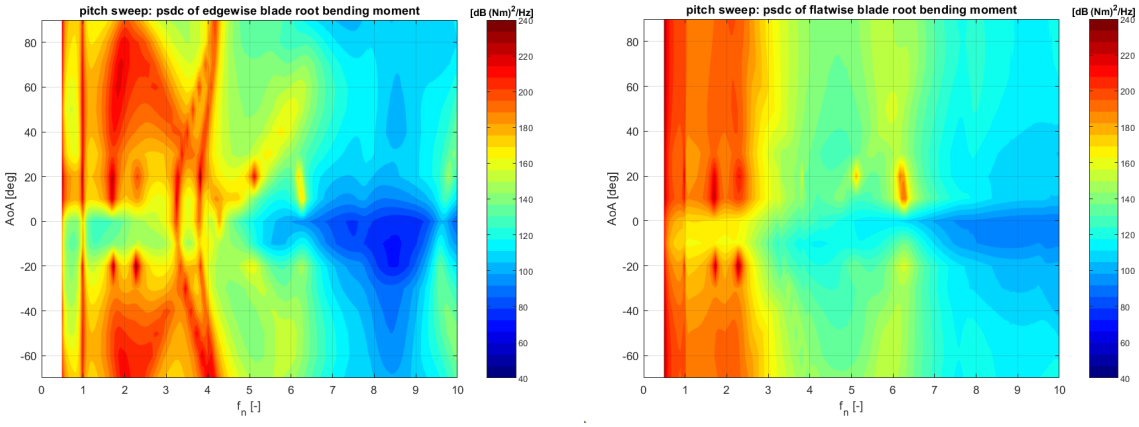

Figure 11: Power spectral density contour of the edgewise (left) and the flatwise (right) blade root bending moments

4.4 Discussion

Most of the observed low damping areas can be attributed to stall. Stall behavior can be described using a static (airfoil polars) and the dynamic contribution [13, 14, 15], which both inhibit a level of uncertainty. The possible resonances are a combination of system natural frequencies and the vortex shedding excitation, which is a complex flow phenomena that depends on many conditions (operational, but also higher order effects such as 3D flow [16]) and requires higher fidelity models to be captured. Despite the uncertainty on the exact response in the field, some areas of interest have been identified from the modal and spectral analysis using a low fidelity model. This can be used to steer further analysis or dedicated experiments.

5 Conclusions and recommendations

Wind turbine vibrations at standstill are observed at high wind speeds. The experimental data from the TIADE field campaign, including unique pressure measurements, are a valuable source to enhance our understanding about the conditions and sources of excitation causing these vibrations. Utilizing a parked 3.8 MW research turbine a dedicated test at different pitch and yaw angles and rotor positions was performed at standstill. The measurements were done for wind speeds of at least 15 m/s.

The pitch and yaw traverse are well suited for a spectral analysis to extract many relevant vibration frequencies of the turbine. In two test campaigns severe vibrations of the wind turbine were observed. Analyzing the spectra of the pressure sensors do not indicate the presence of a dominant vortex shedding frequency at the blade resulting in vortex-induced vibrations.

Recommendations for future experiments could include the instrumentation of multiple cross-sections

to investigate differences in local vortex-shedding frequencies and whether particular cross-sections are driving the occurrence of vortex-induced vibrations.

The numerical analysis using a low order model derived with TURBU indicated potential areas of vibration issues due to low damping and resonance. The predicted response under realistic conditions shows similar trends as observed from the measurements. Given the large influence of (dynamic) stall, the effect of model uncertainty (static and dynamic airfoil polars) should be further investigated. The experimental data from the TIADE field campaign, including unique pressure measurements, are a valuable source for this.

6 Acknowledgements

The work conducted in this study is part of the TIADE (Turbine Improvements for Additional Energy). TIADE has been co-financed with Topsector Energiesubsidie from the Dutch Ministry of Economic Affairs under grant no. TEHE119018. LM Wind Power/GE is thanked for providing the data.

References

[1] Den Hartog J 1984 *Mechanical Vibrations* 4th ed (Dover)

[2] Petersen J T, Madsen H A, Björck A, Enevoldsen P, Øye S, Ganander H and Winkelaar D 1998 Prediction of dynamic loads and induced vibrations in stall Tech. rep. Risø National Laboratory URL `https://orbit.dtu.dk/en/publications/prediction-of-dynamic-loads-and-induced-vibrations-in-stall`

[3] Fung Y 2008 *An Introduction to the Theory of Aeroelasticity* Dover Books on Aeronautical Engineering (Dover Publications) ISBN 9780486469362 URL `https://books.google.nl/books?id=nic3DwAAQBAJ`

[4] Bouwmeesters M 2023 *Stall and vortex induced vibrations in large wind turbines* Master's thesis TU Delft, Aerospace Engineering URL `https://repository.tudelft.nl/record/uuid:b553974f-bba6-4f06-a81e-5eed141bfdf8`

[5] Khan M A, Ferreira C S, Schepers G J and Sørensen N N 2020 *Wind Energy* **23**(1) 31–44 ISSN 10991824

[6] Chen C, Zhou J W, Li F and Zhai E 2022 *Renewable Energy* **187** 710–727 ISSN 18790682

[7] IEC 2005 61400-1 ed.3: Wind turbines - part 1: Design requirements Standard International Electrotechnical Commission Geneva URL `https://webstore.iec.ch/publication/29360`

[8] Fritz E, Boorsma K, Caboni M and Herrig A 2024 *Wind Energy* **27** 1483–1498 ISSN 1095-4244, 1099-1824 URL `https://onlinelibrary.wiley.com/doi/10.1002/we.2952`

[9] Pergod L, Fritz E, Boorsma K and Savenije F 2024 Aeroelastic model of the TIADE turbine techreport TNO 2024 R1221 TNO

[10] Xu G, Yu W, Sciacchitano A and Ferreira C S 2025 *Wind Energy* **28** URL `https://onlinelibrary.wiley.com/doi/10.1002/we.2974`

[11] van Engelen T 2007 Control design based on aero-hydro-servo-elastic linear models from TURBU (ECN) *Proceedings of the European Wind Energy Conference (EWEC), Milan, 2007*

[12] Savenije F J and Peeringa J M 2009 Aero-elastic simulation of offshore wind turbines in the frequency domain, TURBU@Sea techreport ECN-E–09-060 Energy research Centre of the Netherlands

[13] Snel H 1997 Heuristic modelling of dynamic stall characteristics *Proceedings of the European Wind Energy Conference* (Dublin, Ireland) pp 429–433

[14] Holierhoek J, de Vaal J, van Zuijlen A and Bijl H 2013 *Wind Energy* 139–158

[15] Adema N, Kloosterman M and Schepers J 2020 *Wind Energy Science* 577–590

[16] Heinz J, Sørensen N, Zahle F and Skrzypiński W 2016 *Wind Energy* **19**(11) 2041–2051 ISSN 10991824